Biphoton manipulation with a fiber-based pulse shaper

Joseph M. Lukens,[1] Amir Dezfooliyan,[1] Carsten Langrock,[2] Martin M. Fejer,[2]
Daniel E. Leaird,[1] and Andrew M. Weiner[1,*]

[1]School of Electrical and Computer Engineering, Purdue University, West Lafayette, Indiana 47907, USA

[2]E. L. Ginzton Laboratory, Stanford University, Stanford, California 94305, USA

*Corresponding author: amw@purdue.edu

Received July 22, 2013; revised September 27, 2013; accepted October 6, 2013;
posted October 8, 2013 (Doc. ID 194429); published November 7, 2013

We demonstrate spectral shaping of entangled photons in the telecom band with a programmable, fiber-based optical filter. The fine-resolution spectral control permits implementation of length-40 Hadamard codes, through which we are able to verify frequency anticorrelation with a 20-fold increase in total counts over that permitted by the equivalent pair of monochromators at the same input flux. By programming the complex spectral transmission function corresponding to a Mach–Zehnder interferometer, we also construct variations on Franson interferometers that are free from mechanical instabilities, demonstrating spectral phase independence in the slow-detector limit, in which all temporal features are unobservable. Our configuration furnishes a single, compact arrangement for manipulating telecom biphotons and characterizing their quality.

OCIS codes: (270.5565) Quantum communications; (320.5540) Pulse shaping.
http://dx.doi.org/10.1364/OL.38.004652

Entangled photons have proven themselves indispensable in the experimental realization of quantum mechanics. Not only have they found use in testing quantum paradoxes such as Bell's inequality [1], they have also assumed central roles in quantum key distribution and quantum teleportation [2]. Independently, Fourier pulse shaping has engendered unparalleled control of classical optical waveforms, with applications ranging from coherent control of light-matter interactions to radio-frequency photonics [3]. And although initial work in pulse shaping was concerned with coherent classical sources, it has also been applied to manipulate the electric field cross-correlation of incoherent classical light [4] and more recently to shape the correlation function of entangled photons [5]. Since then, there have been relatively few experiments exploring biphoton shaping with spatial light modulators (e.g., [6–8]), and thus there remains much untapped potential. In this work, we demonstrate spectral shaping of entangled photons in the telecommunications band around 1550 nm, which to our knowledge represents the first time biphotons of this frequency have been shaped by spatial light modulators. Our configuration integrates into existing fiber-based systems and therefore proves valuable for photon sources used in quantum communication over optical fiber.

Our entangled photons are generated via spontaneous parametric downconversion (SPDC) [9,10], in which a high-frequency pump photon decays into two daughter photons; individually, each generated photon can be extremely broadband, yet the sum of their two measured frequencies must equal that of the pump. The nonlinear medium we employ is a highly efficient periodically poled lithium niobate (PPLN) waveguide [11–13]. Figure 1(a) shows the experimental setup. We couple a continuous-wave pump laser into a PPLN waveguide heated to 140°C. At this temperature, degenerate downconversion is phase-matched for a pump wavelength of ~774 nm. After passing through colored glass filters to remove residual pump light, the entangled photons generated around 1548 nm are then coupled into optical fiber and sent through a pulse shaper. We use the commercial Finisar WaveShaper 4000S/X, which offers independent amplitude and phase control at 20 GHz resolution over the band from 1527 to 1600 nm—corresponding in total to 450 resolvable spectral regions—in addition to the capability to send each frequency to one of four output ports. This allows us to split the two photons by wavelength, with the high-frequency "signal" photon exiting one output port and the corresponding "idler" leaving another. Similar wavelength splitting of entangled photons has been demonstrated previously with a wavelength-selective switch [14]; here we augment this capacity with the inclusion of programmable pulse shaping. After wavelength demultiplexing, the photons are then detected on a pair of gated InGaAs single-photon avalanche photodiodes (Aurea SPD_AT_M2), operated at 20% quantum efficiency and with a 10 ns gate clocked at 1.25 MHz. The photon arrivals are tagged by an event timer (HydraHarp 400), with coincidences defined as detections within 1 ns of each other.

With approximately 10 mW of pump light in the waveguide, we couple about 80 nW of SPDC photons into optical fiber. The spectrum immediately following the collimator is shown in Fig. 1(b), acquired at a resolution of 250 GHz: the SPDC emission has a 3 dB bandwidth of

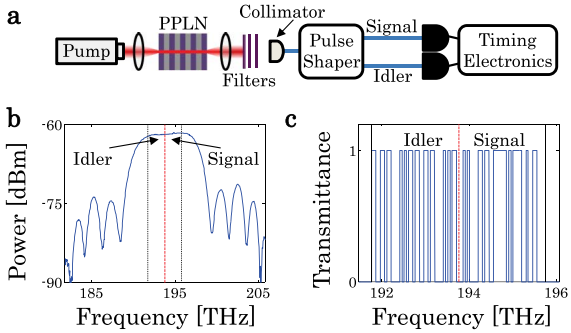

Fig. 1. (a) Experimental setup. (b) SPDC spectrum after collimator, showing signal and idler passbands. The total FWHM is 7.5 THz. (c) Pulse-shaper transmittance for Hadamard codes. Here code 8 is applied to the idler spectrum and code 30 to the signal.

7.5 THz and is nearly flat over the 4 THz band set for the pulse shaper. For subsequent tests with the InGaAs detectors, we attenuate the pump beam to minimize accidentals caused by multipair generation; for the following experiments, we operate at single detector count rates around 3500 s^{-1} for 2 THz signal and idler passbands and flat phase on the pulse shaper.

To verify spectral entanglement, we exploit a Hadamard-based approach made possible by the programmability and fine spectral resolution of our pulse shaper. Conceptually, the most straightforward way to demonstrate entanglement would instead be to compare the coincidences between two narrow slits on a spectrometer; only when the slits are evenly spaced about the entanglement frequency would coincidences be registered. And indeed, a pulse shaper is well suited for such a measurement, as the "two slits" can be implemented simply by programming narrow spectral filters. However, this technique suffers from a low signal-to-noise ratio, since the slit width is directly proportional to the probability that a given photon passes. For example, in an experiment with N frequency bins, each equal to $1/N$ of the total signal (or idler) bandwidth, coincidences between symmetric passbands would drop to $1/N$th the number of coincidences when all slits are open. As we show below, we can obtain an $N/2$-fold increase in coincidences at a given spectral resolution and input flux with an approach analogous to classical Hadamard spectroscopy [15].

In this work we use modified Walsh–Hadamard codes as spectral filters. A standard Walsh–Hadamard family consists of a set of N length-N sequences of 1's and −1's (or equivalently phases of 0 and π), with the property that any two codes are orthogonal [16]. Since we consider amplitude coding here, we replace all π-phase elements with zero-transmissivity chips, yielding modified codes containing 1 and 0's instead. (As we show later, our slow detectors are intrinsically insensitive to any spectral phase modulation.) In this scheme, the signal photon is encoded with one such amplitude sequence, and the idler is decoded with another. Figure 1(c) provides an example code pair. With 80 resolvable spectral elements, these codes possess greatly increased complexity over previous biphoton phase and amplitude functions [5–7], made possible here by the pulse-shaper resolution. Due to signal-idler spectral anticorrelation, a large number of simultaneous detections are registered when the codes are matched (perfectly symmetric about the degeneracy point), since the signal photon corresponding to a given idler detection is always passed. On the other hand, when the codes are mismatched, only half of the partner signal photons are passed. Thus pure spectral anticorrelation is verified by an ideal 2:1 contrast between matched and mismatched codes.

This precise factor of 2 stems from the defining characteristics of Hadamard codes. In mismatched cases, one half of the 1's on one code must multiply 1's on the partner, while the other half multiply 0's. Excluding the code consisting of all 1's, each sequence in a Hadamard family contains precisely $N/2$ 1's and $N/2$ 0's, and so matched codes yield a total of $N/2$ passed signal-idler bins, whereas mismatched codes give only $N/4$ pair combinations that are simultaneously open. And since the equivalent monochromator passes only one bin at a time, the detected coincidence rate is $N/2$ times lower for a given resolution and input flux. Comparing our length-40 Hadamard approach to the equivalent two-slit test, then, we are able to increase the total coincidence rate 20-fold for our chosen spectral resolution and input flux. Admittedly, with the ability to raise the biphoton flux by a factor of $N/2$, it would be possible to achieve the same coincidence rate for matched monochromators as in our Hadamard approach. However, in addition to the requirement of adjusting the pump power, which may be impractical in some circumstances, doing so also increases the relative probability for accidentals due to multiple-pair generation, which scales quadratically with the pair flux [17]. In contrast, our method boosts the coincidence rate at any given pump power, significantly improving sensitivity without altering the statistical properties of the input field. Hadamard coding can thereby be viewed as a source-independent method to verify spectral entanglement much more efficiently than comparing the coincidences between two narrowband filters.

The results of this experiment are presented in Fig. 2. Each point was obtained over a 30 s integration time, and the average contrast between matched and mismatched codes is 1.89:1, compared to the theoretical maximum of 2:1 for perfectly flat spectra and no accidentals. The relatively low rate of coincidences per idler detection is due to the optical loss of the system, particularly the approximately 6 dB pulse-shaper insertion loss, which proves to be the primary limitation of our configuration.

The utility of this pulse-shaper arrangement is further highlighted by experiments in Franson interferometry. In the typical Franson setup [Fig. 3(a)], entangled photons are sent through separate Mach–Zehnder interferometers (MZIs), identical except for phase shifts in their long arms, with detectors placed at one of the output ports of each MZI [18]. When the path-length difference between MZI arms exceeds the broadband one-photon coherence length, but is less than that of the pump,

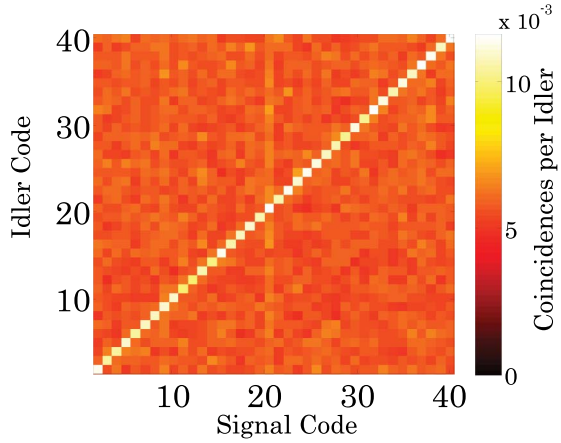

Fig. 2. Coincidence rate as a function of signal-idler Hadamard codes, normalized to idler detections. Only codes 2 through 40 are shown, as code 1 corresponds to full transmission. When the codes are matched, approximately twice as many coincidences are registered as when the codes differ, confirming spectral entanglement.

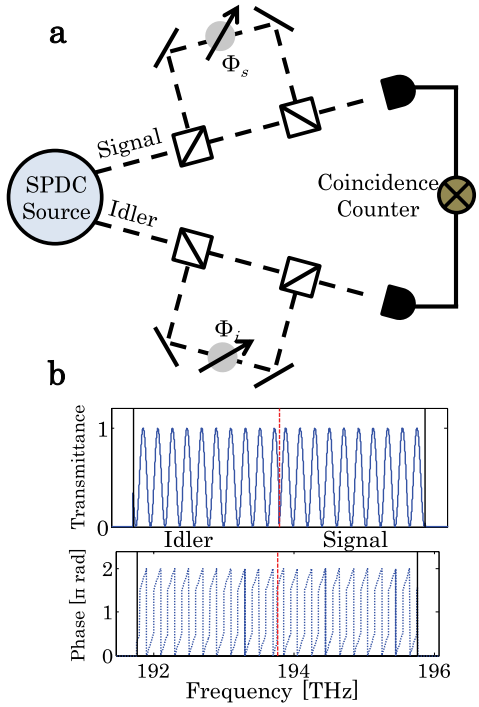

Fig. 3. (a) Typical Franson interferometer. The signal and idler photons are sent through MZIs with different phase shifts in the long arms: Φ_s for the signal and Φ_i for idler. (b) Spectral transmittance and phase applied by pulse shaper to emulate a Franson interferometer. Signal and idler photons are distinguished by frequency and sent through spectral filters that are equivalent to traversing MZIs. In addition to 2π jumps from wrapping the spectral phase, π discontinuities also occur as the sinusoidal field transmission function—the square of which gives the power transmittance—changes sign.

the coincidences between the two detectors display interference even though single-photon interference is absent. The measured coincidence rate R_c can be expressed mathematically as

$$R_c \propto 1 + \mathcal{V}\cos(\Phi_s + \Phi_i + 2\omega_0 T), \tag{1}$$

where Φ_s and Φ_i are the phase shifts experienced in the long arms of the signal and idler MZIs, respectively; $2\omega_0$ is the pump frequency; T is the relative delay between long and short arms; and $\mathcal{V}$ is the visibility. When the detector resolution is sufficiently fine to distinguish between photon arrivals separated in time by an amount T, the visibility can reach 1, whereas when this is not the case, the maximum possible value is 0.5 [19].

Since an MZI transforms the input optical field in a manner that is linear and time-invariant, the field at each output port can be viewed as the result of applying a complex spectral filter function to the input. This allows us to use the pulse shaper to emulate each MZI by programming the appropriate spectral phase and amplitude [7]. Omitting an unimportant overall delay, the spectral transmittance applied to the pulse shaper for the signal MZI is

$$\mathcal{T}(\omega) = \cos^2\left(\frac{\Phi_s + \omega T}{2}\right), \tag{2}$$

and the spectral phase is

$$\phi(\omega) = \begin{cases} (\Phi_s + \omega T)/2 & \text{if } \cos\left(\frac{\Phi_s+\omega T}{2}\right) > 0 \\ (\Phi_s + \omega T)/2 + \pi & \text{if } \cos\left(\frac{\Phi_s+\omega T}{2}\right) < 0. \end{cases} \tag{3}$$

The idler amplitude and phase are obtained by replacing Φ_s with Φ_i. An example filter function for $\Phi_s = \pi/2$, $\Phi_i = 0$, and $T = 5$ ps is given in Fig. 3(b). In replacing the mirrors and beam splitters of a traditional MZI with a stand-alone pulse shaper, our implementation offers enhanced stability over the standard Franson arrangement. Unlike mounted mirrors which destroy interference at the slightest mechanical perturbation, this pulse shaper provides a constant spectral filter independent of table vibrations or temperature fluctuations.

Programming $T = 5$ ps and sweeping the phase applied to the pulse shaper, we obtain the results of Fig. 4(a), which reveal an interference visibility of around 0.43. The pulse shaper's time aperture—or the time window over which it can accurately reproduce the programmed waveform—is ~30 ps, whereas the detector resolution is ~200 ps, so 0.5 is the largest visibility possible in the current arrangement. And if we allow for the possibility that the long-arm delays of the two MZIs are not identical but differ by an amount ΔT, the coincidence rate for a flat signal spectrum of width $\Delta\omega$ assumes the form

$$R_c \propto 1 + \mathcal{V}\,\mathrm{sinc}\left(\frac{\Delta\omega\Delta T}{2}\right)\cos(\Phi_s + \Phi_i + \varphi), \tag{4}$$

where φ is some constant phase offset. Thus our interference visibility is expected to reduce like a sinc function.

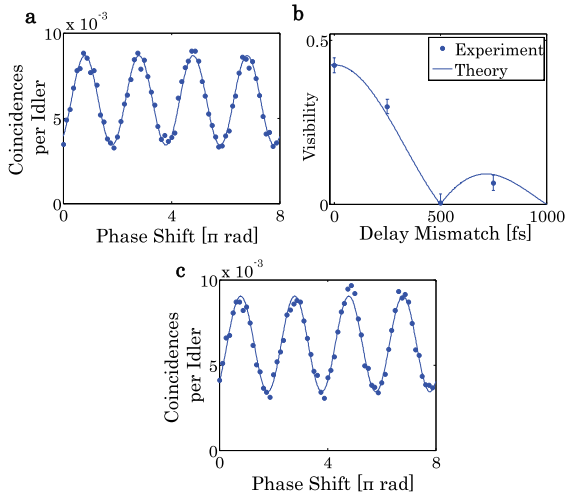

Fig. 4. (a) Experimental coincidence rate for pulse-shaper Franson interferometer, at matched MZI delays and with a 30 s integration time per point. The detected coincidences show interference with the applied phase $\Phi_s + \Phi_i$, possessing a visibility of 0.43. (b) Reduction in visibility as the MZI delays are shifted from each other. The theoretical curve is scaled to match the experimental visibility at zero mismatch, and error bars represent 95% confidence intervals for the fit parameters. (c) Coincidence rate for pulse-shaper interferometer with flat spectral phase, again at a measurement time of 30 s per data point. The visibility is 0.45.

The effect of programming delay mismatch between the two MZIs on the measured visibility is presented in Fig. 4(b), confirming theoretical considerations.

The pulse shaper also permits the creation of "interferometers" with no mechanical analogues, an example of which was examined previously in the phase-sensitive ultrafast detection regime [7]. Here we extend these concepts to the slow-detector limit, in which we show that spectral phase has no effect. For example, if we apply the spectral amplitude of Fig. 3(b), but instead impose flat phase, we anticipate the same interference pattern as with true MZIs. To understand this general result, consider a biphoton spectrum described by the complex weight function $F(\Omega)$, where Ω gives the signal frequency offset from ω_0. Signal filter $H_s(\omega)$ and idler filter $H_i(\omega)$ are applied to the entangled photons, and coincidences are measured. In the slow-detector limit, the measured coincidence rate R_c is given by [14]

$$R_c \propto \int_{-\infty}^{\infty} d\Omega |F(\Omega) H_s(\omega_0 + \Omega) H_i(\omega_0 - \Omega)|^2. \quad (5)$$

Therefore the measured coincidence rate is independent of spectral phase in this limit. Intuitively, this result makes sense, for it states that the total coincidence rate is an integral over all entangled frequency combinations, with each pair multiplied by the probabilities both photons are passed. We confirm this phase independence experimentally by applying the transmission functions of Eq. (2), but with flat phase instead of Eq. (3); the result is given in Fig. 4(c). With a visibility of about 0.45, the coincidence rate is nearly identical to the true MZI simulator of Fig. 4(a). We emphasize that this independence on spectral phase is only valid when the detector resolution τ_d satisfies $\tau_d \gg T$. When $\tau_d \ll T$, flat spectral phase does not produce the unity visibility possible with true MZI phase.

We have experimentally verified a simple, fiber-pigtailed pulse-shaping system for the control of entangled photons in the telecom band, which offers integrability with existing fiber-based quantum systems. Our arrangement is immediately useful as a programmable optical simulator to test biphoton sources in a stable, straightforward configuration.

This project was funded by the Office of Naval Research under grant no. N000141210488. J. M. L. acknowledges financial support from the Department of Defense through a National Defense Science and Engineering Graduate Fellowship.

References

1. A. Aspect, Nature **398**, 189 (1999).
2. N. Gisin and R. Thew, Nat. Photonics **1**, 165 (2007).
3. A. M. Weiner, Opt. Commun. **284**, 3669 (2011).
4. V. Binjrajka, C.-C. Chang, A. W. R. Emanuel, D. E. Leaird, and A. M. Weiner, Opt. Lett. **21**, 1756 (1996).
5. A. Pe'er, B. Dayan, A. A. Friesem, and Y. Silberberg, Phys. Rev. Lett. **94**, 073601 (2005).
6. B. Dayan, Y. Bromberg, I. Afek, and Y. Silberberg, Phys. Rev. A **75**, 043804 (2007).
7. F. Zäh, M. Halder, and T. Feurer, Opt. Express **16**, 16452 (2008).
8. E. Poem, Y. Gilead, Y. Lahini, and Y. Silberberg, Phys. Rev. A **86**, 023836 (2012).
9. L. Mandel and E. Wolf, *Optical Coherence and Quantum Optics* (Cambridge University, 1995).
10. Y. Shih, Rep. Prog. Phys. **66**, 1009 (2003).
11. K. R. Parameswaran, R. K. Route, J. R. Kurz, R. V. Roussev, M. M. Fejer, and M. Fujimura, Opt. Lett. **27**, 179 (2002).
12. C. Langrock, S. Kumar, J. E. McGeehan, A. E. Willner, and M. M. Fejer, J. Lightwave Technol. **24**, 2579 (2006).
13. S. Tanzilli, H. De Riedmatten, W. Tittel, H. Zbinden, P. Baldi, M. De Micheli, D. B. Ostrowsky, and N. Gisin, Electron. Lett. **37**, 26 (2001).
14. J. Oh, C. Antonelli, and M. Brodsky, J. Lightwave Technol. **29**, 324 (2011).
15. E. D. Nelson and M. L. Fredman, J. Opt. Soc. Am. **60**, 1664 (1970).
16. K. G. Beauchamp, *Applications of Walsh and Related Functions* (Academic, 1984).
17. C. Liang, K. F. Lee, M. Medic, P. Kumar, R. H. Hadfield, and S. W. Nam, Opt. Express **15**, 1322 (2007).
18. J. D. Franson, Phys. Rev. Lett. **62**, 2205 (1989).
19. Z. Y. Ou, X. Y. Zou, L. J. Wang, and L. Mandel, Phys. Rev. Lett. **65**, 321 (1990).